UNIVERSITY OF OKLAHOMA

GRADUATE COLLEGE

TIME-DEPENDENT DENSITY FUNCTIONAL THEORY STUDIES

OF CHARGE TRANSFER IN OXYGEN DISSOCIATION

ON SILVER NANOPARTICLE

A THESIS

SUBMITTED TO THE GRADUATE FACULTY

in partial fulfillment of the requirements for the

Degree of

MASTER OF SCIENCE

By

JINGHENG DENG
Norman, Oklahoma
2020

TIME-DEPENDENT DENSITY FUNCTIONAL THEORY STUDIES
OF CHARGE TRANSFER IN OXYGEN DISSOCIATION
ON SILVER NANOPARTICLE

A THESIS APPROVED FOR THE
DEPARTMENT OF CHEMISTRY AND BIOCHEMISTRY

BY THE COMMITTEE CONSISTING OF

Dr. Yihan Shao, Chair

Dr. Bin Wang

Dr. Wak Tak Yip

Acknowledgements

First, I wish to express my gratitude to my research advisor, Professor Yihan Shao, for teaching me a great deal of quantum chemistry, for encouraging to explore and work in quantum chemistry, for his guidance and unconditional support during all these years of graduate school, and for being an excellent mentor. I am grateful for having had the opportunity to work with him.

I also wish to thank my friends, Junjie Yang and Zheng Pei, for the helpful discussions, suggestions and support during the writing of this thesis.

Abstract

We performed calculations to study the dominating charge transfer mechanism in an plasmon-mediated catalytic reaction, oxygen dissociation on Ag nanoparticles (NPs) by using time-dependent density functional theory. Two mechanisms, plasmon-induced hot-electron transfer (PHET) and direct interfacial charge transfer (DICT), were discussed. In order to study the effects of the size and shape of nanoparticles on the charge transfer, ten different geometries of Ag-NP-O_2 were considered. Real-time time-dependent density functional theory (RT-TDDFT) was used to obtain the evolution of electron density and energy. And fragment based Hirshfeld (FBH) population and Becke population were calculated to analyze the evolution of electron density and energy on the oxygen molecule. Linear-response time-dependent density functional theory (LR-TDDFT) calculations and natural transition orbitals (NTOs) analysis were performed to provide insights into the charge transfer process. The results of RT-TDDFT and LR-TDDFT are consistent with each other. It can be concluded that the PHET mechanism is the one dominating the charge transfer process while the DICT mechanism only has limited contribution.

Table of Contents

Chapter 1

Introduction

1.1 Overview

A plasmon is a quantized collective oscillation of free electron gas in a metal, typically including Au and Ag, when the excitation is induced by the incident electromagnetic radiation[1]. Plasmonic nanoparticles are small particles whose sizes are far smaller than the wavelengths of incident radiations and it enables these particles to couple the electron gas oscillation with the radiations[2]. When radiation is applied on the surface of plasmonic nanoparticles with high free electron mobility and if the energy of radiation matches the resonance energy of the oscillation of surface valence electrons, localized surface plasmon resonance (LSPR) excitation will occur[3]. The resonance between radiation and the surface electrons can lead to the formation of coherent electrons in space and energy. As a result, LSPR excitation will produce a strong electric field, which is localized on the surface of the nanoparticles. The decay of the electric field further can lead to the formation of energetic charge carriers, hot electrons and holes[4, 5, 6]. Thus, plasmonic nanoparticles have attracted people's attention for several decades due to the great potential application in photochemical catalysis [7, 8, 9, 10]. When a molecule is

adsorbed on the surface of plasmonic nanoparticles, the hot electrons or holes can transfer to the adsorbate and further result in the formation of ionized adsorbate. It can be applied in catalyzing reaction, which is known as plasmonic-mediated catalysis by creating ionized unstable intermediates through LSPR. Typical examples include H_2O splitting, CO oxidation, hydrogenation of carbonyls, H_2 and O_2 dissociation, etc[7, 9, 11, 12].

1.2 Plasmon-mediated Catalysis

The idea of plasmon-mediated catalysis is to utilize the strong electric field generated due to the decay of excited plasmon to inject charge carriers into the virtual orbitals of reactants adsorbed on the surface of noble metals and eventually form an unstable ionic transition state of reactants.[9] Therefore, the formation of activated reactant depends on the generation of hot charge carriers (electrons or holes) which follows by the decay of plasmon excitation.

In plasmonic photocatalysis, electron-hole separation plays an essential role to activate the reaction. Therefore, the mechanism of electron-hole separation becomes the key to design a high-efficiency catalysis strategy. There are two reported mechanisms: conventional plasmon-induced hot-electron transfer (PHET) and direct interfacial charge transfer (DICT)[13, 14]. For a metal-adsorbate complex, the conventional PHET mechanism indicates that the electrons are excited from the occupied orbitals to the virtual orbitals at the metal. This is followed by electron-electron scattering (Landau damping), which leads to transferring the excited electrons from the conduction band of the metal to the virtual orbitals of the adsorbate. While in the DICT mechanism, charge carriers (electrons) can directly transfer from the occupied metal orbitals to the virtual adsorbate orbital through

chemical interface damping (CID)[14, 15, 16, 17]. Foerster et al. reported that the contribution of CID depends on the size of nanoparticles and predicted that CID is the dominant mechanism for plasmon decay process occurring in small gold nanorods[18]. Recent studies are paying more and more attention to the DICT mechanism for its potentially promising application on selective catalysis.[9] In the DICT mechanism, by tuning the shape and size of noble metal nanoparticles as well as the incident radiation, it is possible to improve the reaction efficiency and selectivity by selectively control the formation of the particular products through depositing energy in the corresponding reaction coordinate[3].

Recently, plasmon-mediated O_2 dissociation catches many researcher's attention[19, 20, 21, 22, 23]. Linic et al. reported plasmon-driven O_2 dissociation reaction on Ag nanotubes [24]. Wu et al. demonstrated a strategy of plasmon-induced hot electrons enhancement to catalyze oxygen reduction reaction on non-noble metal[25]. Even though plasmon-mediated O_2 dissociation reaction has generated a lot of interest, the electron transfer mechanism at molecular level still remains unclear.

1.3 Theoretical Methods

In practical applications, in order to design an appropriate reaction pathway to obtain desired products, it is important to determine which mechanism is dominating the reaction at molecular level.

In addition to experimental exploration on the mechanism of plasmonic mediated catalytic reaction, theoretical studies can also play an important role in studying the plasmon behavior of noble metal nanoparticles. Zhao et al. built a pyriding-Ag_{20} model to study surface-enhanced Raman scattering[26]. Li et al. applied real-time time-dependent density functional theory to estimate the exciton trans-

fer and decay in a Ag nanowire array [27]. Yan et al. showed that the electron transition between the monolayer of hydrogen and the silver(111) surface can be modeled with using linear-response time-dependent density functional theory[28]. Since the computational cost increases significantly with the size of system ($\mathcal{O}(n^4)$ for LR-TDDFT, $\mathcal{O}(n^2)$ for RT-TDDFT), studying a smaller system can be a good starting point. Kummel et al. and Aikens et al. performed calculations on different sizes of noble metal nanoparticles and showed that the resulting absorption spectra of smaller nanoparticles exhibit similar characteristic peaks compared to the larger nanoparticles[29, 30, 31, 32, 33, 34]. As a result, the plasmon modes of different sizes of nanoparticles are expected to be similar.

This thesis focuses on the charge transfer mechanism for O_2 dissociation reaction on Ag nanoparticles using real-time time-dependent density functional theory (RT-TDDFT) and linear-response time-dependent density functional theory (LR-TDDFT). Both methods are essentially equivalent but each one also has its own unique features. For RT-TDDFT, the major feature is that the electronic dynamics can be obtained directly, which can provide an intuitive picture of electron behavior. However, to obtain a complete and accurate picture of the process, it requires a sufficiently long simulation with an appropriate time step, which can be as small as 0.02 atomic unit (0.5 attosecond). This could make the calculation very expensive. For LR-TDDFT, on the other hand, it is much more efficient than RT-TDDFT. Compared with RT-TDDFT, the low-lying excited states can be obtained with a relative low computational cost.Due to this reason, LR-TDDFT has been implemented in most of mainstream quantum chemistry calculation packages. Besides, various analysis methods for LR-TDDFT can be done in most of packages to obtain the insights on electron excitation, including natural transition

orbitals analysis, detachment/attachment density analysis[35].

In the remainder of this introduction, we briefly introduce the key concepts of two methods used in this study, RT-TDDFT and LR-TDDFT. Further discussions about the analysis techniques and calculation details will be discussed in chapter Two. Results will be presented in Chapter Three. Conclusions will be included in Chapter Four.

1.4 Density Functional Theory (DFT)

Density functional theory was established by Walter Kohn and Pierre Hohenberg in 1964[36] and then further developed by Walter Kohn and Lu Jeu Sham in 1965[37] to make it become practical. For a N-particle system, the Schödinger equation is written as:

$$\hat{H}\Psi(\mathbf{r}_1, \mathbf{r}_2, \mathbf{r}_3, ..., \mathbf{r}_{N-1}, \mathbf{r}_N) = E\Psi(\mathbf{r}_1, \mathbf{r}_2, \mathbf{r}_3, ..., \mathbf{r}_{N-1,}, \mathbf{r}_N) \tag{1.1}$$

with Hamiltonian:

$$\hat{H} = -\frac{1}{2}\sum_i \nabla_i^2 + \sum_{i\neq j} \frac{1}{|\mathbf{r}_i - \mathbf{r}_j|} + \sum_i v_{ext}(\mathbf{r}_i) \tag{1.2}$$

where $\Psi(\mathbf{r}_1, \mathbf{r}_2, \mathbf{r}_3, ..., \mathbf{r}_{N-1}, \mathbf{r}_N)$ is the wave function of all electrons at positions $\mathbf{r}_1, \mathbf{r}_2, \mathbf{r}_3, ..., \mathbf{r}_{N-1}, \mathbf{r}_N$ and $v_{ext}(\mathbf{r})$ is the external potential which includes the coulomb potential caused by nucleus.

The energy of electrons is given by:

$$E = \int \cdots \int \Psi^* \hat{H} \Psi d\mathbf{r}_1 \cdots d\mathbf{r}_N$$

$$= \int \cdots \int \Psi^* \left(-\frac{1}{2} \sum_i \nabla_i^2 \right) \Psi d\mathbf{r}_1 \cdots d\mathbf{r}_N$$

$$+ \int \cdots \int \Psi^* \left(\sum_{i \neq j} \frac{1}{|\mathbf{r}_i - \mathbf{r}_j|} \right) \Psi d\mathbf{r}_1 \cdots d\mathbf{r}_N$$

$$+ \int \cdots \int \Psi^* \left(\sum_i v_{ext}(\mathbf{r}_i) \right) \Psi d\mathbf{r}_1 \cdots d\mathbf{r}_N \tag{1.3}$$

Within Kohn-Sham DFT, the wave function Ψ of a non-interacting system can be expressed in the form of Slater determinant with a set of orthonormal molecular orbitals $\{\psi_i\}$:

$$\Psi_{non-inter} = \frac{1}{\sqrt{N!}} \begin{vmatrix} \psi_1(\mathbf{x}_1) & \psi_2(\mathbf{x}_1) & \psi_3(\mathbf{x}_1) & \ldots & \psi_N(\mathbf{x}_1) \\ \psi_1(\mathbf{x}_2) & \psi_2(\mathbf{x}_2) & \psi_3(\mathbf{x}_2) & \ldots & \psi_N(\mathbf{x}_2) \\ \vdots & \vdots & \vdots & \ddots & \vdots \\ \psi_1(\mathbf{x}_N) & \psi_2(\mathbf{x}_N) & \psi_3(\mathbf{x}_N) & \ldots & \psi_N(\mathbf{x}_N) \end{vmatrix} \tag{1.4}$$

Define electron density:

$$\rho(\mathbf{r}) = \sum_i^{N_{MO}} |\psi_i|^2 \tag{1.5}$$

where ψ_i are the occupied molecular orbitals. Therefore, the total energy then can be written as:

$$E[\rho] = T[\rho] + V_{ee}[\rho] + \int \rho(\mathbf{r}) v_{ext} d\mathbf{r} \tag{1.6}$$

By doing the variation to $E[\rho]$:

$$\frac{\partial E[\rho]}{\partial \rho(\mathbf{r})} = 0 \tag{1.7}$$

The ground state density ρ can be obtained.

Based on eq. 1.5, Kohn and Sham made a further step to improve the accuracy of DFT. They proposed to construct a fictitious non-interacting system which has the same density as the real one. The resulting wave functions are fictitious and electronic correlation is not included. By doing so, the kinetic term in eq 1.5 is known so that no approximation on kinetic energy term is needed. Define:

$$E_{xc}[\rho] = T[\rho] - T_s[\rho] + V_{ee}[\rho] - J[\rho] \tag{1.8}$$

where $T_s[\rho] = -\frac{1}{2} \sum_i \langle \psi_i | \nabla^2 | \psi_i \rangle$ is the kinetic energy of non-interacting system, $J[\rho] = \frac{1}{2} \int \int \frac{1}{|\mathbf{r}_1 - \mathbf{r}_2|} \rho(\mathbf{r}_1) \rho(\mathbf{r}_2) d\mathbf{r}_1 d\mathbf{r}_2$.

Therefore, the total energy functional then can be written as:

$$E[\rho] = T_s[\rho] + J[\rho] + E_{xc}[\rho] + \int \rho(\mathbf{r}) v_{ext} d\mathbf{r} \tag{1.9}$$

Then, Kohn-Sham (KS) equation can be written as[38]:

$$-\frac{1}{2} \nabla^2 \psi_i + v_{eff} \psi_i = \epsilon_i \psi_i \tag{1.10}$$

$$v_{eff} = v_{ext} + v_{ee} + v_{xc} \tag{1.11}$$

1.5 Time-Dependent DFT (TDDFT)

DFT is a ground state method, which describes time-independent cases. To study excited states, it should be extended to the time-dependent situation. Under the framework of DFT, there are two approaches, real-time time-dependent DFT (RT-TDDFT) and linear-response time-dependent DFT (LR-TDDFT).

1.5.1 Real-Time TDDFT (RT-TDDFT)

RT-TDDFT was established by Runge and Gross in 1983[39]. They showed that the time-dependent density can be determined uniquely from the effective potential. In other words, it implies that the many-body wave function is equivalent to the density. Therefore, the properties of a given system can be obtained through propagating the density. The time-dependent KS equation can be derived from applying variation to an action A:

$$A = \int dt \, \langle \psi(t) | \, i\frac{\partial}{\partial t} - H(t) \, | \psi(t) \rangle \tag{1.12}$$

which satisfies:

$$\frac{\partial A}{\partial \rho(t)} = 0 \tag{1.13}$$

where $\rho(\mathbf{r}, t) = \sum_i^{N_{occ}} |\psi_i(\mathbf{r}, t)|^2$. Apply the same method described in the previous section, one can finally obtain the time-dependent KS eauation:

$$-\frac{1}{2}\nabla^2 \psi_i(\mathbf{r}, t) + v_{eff}\psi_i(\mathbf{r}, t) = i\frac{\partial}{\partial t}\psi_i(\mathbf{r}, t) \tag{1.14}$$

$$v_{eff}(\mathbf{r}, t) = v_{ext}(\mathbf{r}, t) + v_{ee}(\mathbf{r}, t) + v_{xc}(\mathbf{r}, t) \tag{1.15}$$

Detailed algorithm will be discussed in chapter two.

1.5.2 Linear-Response TDDFT (LR-TDDFT)

Other than propagating the density matrix explicitly, another way to solve RT-KS equation is to apply a weak perturbation to the density matrix to get the corresponding response. Starting with TDSCF equation:

$$i\frac{\partial \mathbf{P}(t)}{\partial t} = [\mathbf{F}(t), \mathbf{P}(t)] \tag{1.16}$$

The perturbated density matrix:

$$\mathbf{P}(t) = \mathbf{P}^{(0)} + \lambda \mathbf{P}^{(1)}(t) \tag{1.17}$$

Since the time dependency of the Fock matrix comes from the density matrix, the resulted Fock matrix:

$$\mathbf{F}(t) = \mathbf{F}^{(0)} + \lambda \mathbf{F}^{(1)}(t) \tag{1.18}$$

By plugging equations 1.17 and 1.18 into 1.16 and solving it, one can finally get the resulting response function[40, 41]:

$$F_{aa}^{(0)}x_{ai} - x_{ai}F_{ii}^{(0)} + \left(f_{ai} + \sum_{bj} \left\{ \frac{\partial F_{ai}}{\partial P_{bj}}x_{bj} + \frac{\partial F_{ai}}{\partial P_{jb}}y_{bj} \right\} \right) P_{ii}^{(0)} = \omega x_{ai} \tag{1.19}$$

$$F_{ii}^{(0)}y_{ai} - y_{ai}F_{aa}^{(0)} - P_{ii}^{(0)} \left(f_{ia} + \sum_{bj} \left\{ \frac{\partial F_{ia}}{\partial P_{bj}}x_{bj} + \frac{\partial F_{ia}}{\partial P_{jb}}y_{bj} \right\} \right) = \omega y_{ai} \tag{1.20}$$

It can be further simplified to:

$$\begin{pmatrix} \mathbf{A} & \mathbf{B} \\ \mathbf{B} & \mathbf{A} \end{pmatrix} \begin{pmatrix} \mathbf{X} \\ \mathbf{Y} \end{pmatrix} = \omega \begin{pmatrix} 1 & 0 \\ 0 & -1 \end{pmatrix} \begin{pmatrix} \mathbf{X} \\ \mathbf{Y} \end{pmatrix} \tag{1.21}$$

where:

$$\mathbf{A}_{ai,bj} = \delta_{ij}\delta_{ab}\left(\epsilon_a - \epsilon_i\right) + (ai|jb) - (ab|ji) \tag{1.22}$$

$$\mathbf{B}_{ai,bj} = (ai|jb) - (ab|ji) \tag{1.23}$$

$$\mathbf{X}_{ai} = x_{ai} \tag{1.24}$$

$$\mathbf{Y}_{ai} = y_{ai} \tag{1.25}$$

In LR-TDDFT:

$$\mathbf{A}_{ai,bj} = \delta_{ij}\delta_{ab}\left(\epsilon_a - \epsilon_i\right) + (ai|bj) + (ai\,|f_{xc}|\,bj) \tag{1.26}$$

$$\mathbf{B}_{ai,bj} = (ai|bj) + (ai\,|f_{xc}|\,bj) \tag{1.27}$$

Chapter 2

Methods

2.1 Propagator

The density matrix at time t_2 is propagated from t_1 by applying a unitary propagator:

$$\mathbf{U}(t_2, t_1) = \mathcal{T} \exp\left(-i \int_{t_1}^{t_2} \mathbf{F}(t)dt\right) \tag{2.1}$$

$$\mathbf{P}(t_2) = \mathbf{U}(t_2, t_1)\mathbf{P}(t_1)[\mathbf{U}(t_2, t_1)]^\dagger \tag{2.2}$$

A small time step is necessary to maintain the numerical stability when propagating the density matrix. In this work, the modified midpoint unitary transform (MMUT) method[42] was employed to propagate the density matrix.

Assume the time step is Δt and start from current time, t_N, with current density matrix $\mathrm{P}(t_N)$ and the one at previous half time step, $\mathrm{P}(t_N - 1/2\Delta t)$, to the next one $\mathrm{P}(t_N + 1/2\Delta t)$:

$$\mathbf{P}(t_N + 1/2\Delta t) = (e^{-i\Delta t \mathbf{F}(t_N)})\mathbf{P}(t_N - 1/2\Delta t)(e^{i\Delta t \mathbf{F}(t_N)}) \tag{2.3}$$

where $F(t_N)$ is the Fock matrix at t_N which can be built from $P(_N)$. Then, the density matrix at $t_N + \Delta t$:

$$\mathbf{P}(t_N + \Delta t) = (e^{-i\Delta t \mathbf{F}(t_N)})\mathbf{P}(t_N + 1/2\Delta t)(e^{i\Delta t \mathbf{F}(t_N)}) \tag{2.4}$$

2.2 Natural Transition Orbitals Analysis

In this study, the goal is to find out which electron transfer mechanism involved in the plasmon mediated catalysis is the dominant one. Therefore, looking at natural transition orbitals (NTOs) can give us essential insights on how the electrons (or holes) transfer during the excitation process[43]. The single particle transition density matrix is defined as

$$T_{ia} = \sum_{\sigma} \langle \Psi_{ex} | c_{i\sigma}^{\dagger} c_{a\sigma} | \Psi_0 \rangle \tag{2.5}$$

where i stands for occupied orbitals and a stands for virtual orbitals, σ is the spin index. The dimension of transition density matrix is $N_{occ} \times N_{vir}$. N_{occ} and N_{vir} are the number of occupied and virtual orbitals respectively.

Now define two unitary matrix $\mathbf{U}$ and $\mathbf{V}$:

$$\mathbf{T}\mathbf{T}^{\dagger} u_i = \lambda_i u_i, \quad i = 1...\mathbf{N}_o \tag{2.6}$$

$$\mathbf{T}^{\dagger}\mathbf{T} v_i = \lambda_i' v_i, \quad i = 1...\mathbf{N}_v \tag{2.7}$$

where u_i, v_i are the eigenvectors of $\mathbf{TT}^\dagger$ and $\mathbf{T}^\dagger\mathbf{T}$ separately, λ_i and λ_i' are the corresponding eigenvalues. Then, we have:

$$\mathbf{U} = (u_1, u_2, ..., u_{N_o}) \tag{2.8}$$

$$\mathbf{V} = (v_1, v_2, ..., v_{N_v}) \tag{2.9}$$

The matrix $\mathbf{U}$ is a unitary transformation from the occupied canonical orbitals to the NTOs which can represent the "holes", while $\mathbf{V}$ transform virtual canonical orbitals to the NTOs which can represent "particles". For those eigenvalues which have the same number, the corresponding NTOs are considered as a pair of "hole" and "particle". For a given pair of eigenvalues λ_i, λ_i', they are the excitation amplitudes of NTOs which reflect the importance of the corresponding NTO pair.

2.3 Partitioning Scheme

To obtain the dynamical picture of electron and energy distribution, two kinds of partitioning schemes were performed: fragment based Hirshfeld (FBH) and Becke scheme. For electron partitioning, the FBH scheme is given by[44]:

$$N_A = -\int d\mathbf{r}\, w_A(\mathbf{r})\rho(\mathbf{r}) + Z_A \tag{2.10}$$

where N_A is the charge located on fragment A, ρ is the electron density of the molecule, Z_A is the nuclear charges on isolated fragment A, and w_A is corresponding weight:

$$w_A = \frac{\rho_A(\mathbf{r})}{\sum_B \rho_B(\mathbf{r})} \tag{2.11}$$

The Becke scheme is given by[45]:

$$N_A^{Becke} = -\int d\mathbf{r}\, w_A(\mathbf{r})\rho(\mathbf{r}) + Z_A \tag{2.12}$$

$$w_A^{Becke} = \frac{P_A(\mathbf{r})}{\sum_B P_B(\mathbf{r})} \tag{2.13}$$

where P_A are cell functions which are polynomials in the distance between nuclei A and grid points $(\mathbf{r})$[46]. To obtain the partitioning of energy, it can be done by replacing the electron density with energy density.
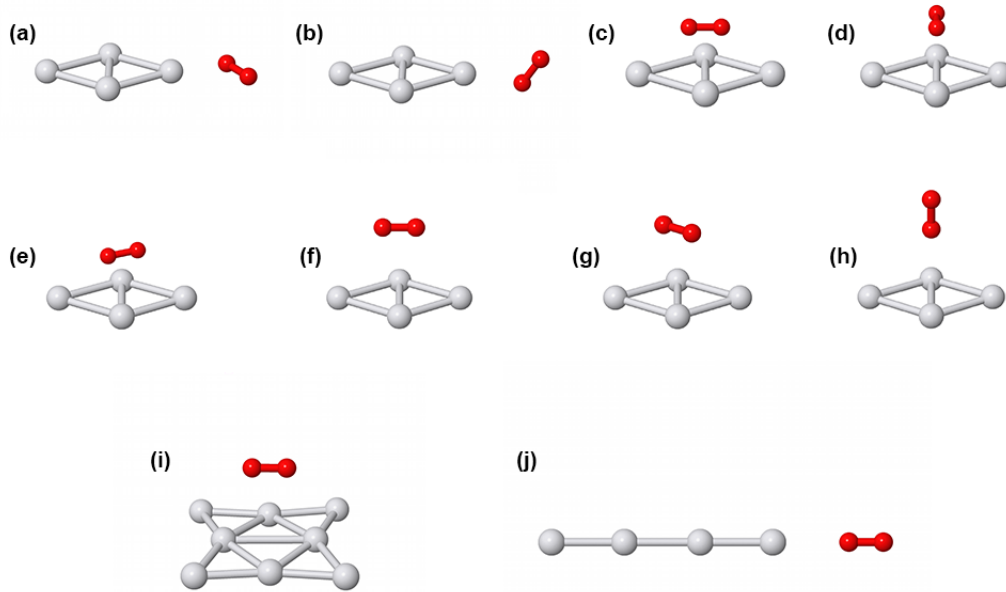
2.4 Calculation Details

Figure 2.1: Optimized geometries studied in this work: a) side-long-short; b) side-long-T; c) side-short-long; d) side-short-short; e) side-short-T; f) parallel-long; g) parallel-short; h) T-shape; i) Ag_8-NC-O_2; j) Ag_4-NW-O_2

In this study, three different types of Ag nanoparticles, Ag_4[47] , Ag_8 nanoclus-

ter (NC) and Ag_4 nanowire (NW)[27, 48] were studied. As shown in Fig. 2.1, the first two rows are the eight configurations of Ag_4 NW O_2 complex, the oxygen molecule was put around the silver cluster with different orientations. In the first two configurations, O_2 was put along the long axis of the Ag_4 and the O-O bond orientation is along the short axis (denoted as "side-long-short") or perpendicular to the plane of Ag_4 (denoted as "side-long-T"). In the next three configurations, O_2 was put along the short axis and the O-O bond orientation is along the short axis (denoted as "side-short-short") or along the long axis (denoted as "side-short-long") or perpendicular to the plane of Ag_4 (denoted as "side-short-T"). In the last three configurations, O_2 was put above the plane of Ag_4 and, according to the orientation of O_2, in parallel with long axis, short axis of Ag_4 and perpendicular to the plane (denoted as "top-parallel-long", "top-parallel-short" and "top-vertical" respectively).For Ag_8-NC-O_2 complex, the oxygen is parallel to the plane of Ag_8. For Ag_4-NW-O_2 complex, all atoms are on a straight line.

Optimization and LR-TDDFT calculations were preformed by using Q-chem 5.1 package[35] with PBE functional[49]. 6-31G(d) basis set was used on oxygen atoms and Stuttgart effective core potential and basis set[50] was used on silver atoms. The same level of theory was used throughout the whole work. In LR-TDDFT calculations, 600 excited states and the corresponding natural transition orbitals (NTOs) were obtained.

The electronic dynamics of all geometries were obtained by performing RT-TDDFT calculations with using PySCF package[51]. The modified Midpoint Unitary Transform (MMUT)[42] propagation scheme was used and three time steps (0.02, 0.05, 0.2 a.u.) were adopted. For all RT-TDDFT calculations, a weak-field perturbation (for Ag_8-NC-O_2 and Ag_4-NC-O_2, the field strength was 10^{-3} a.u.; for Ag_4-NW-O_2,

it was 10^{-4} a.u.) was applied to the initial state in the direction from Ag nanoparticles to O_2 molecule. For all Ag_4 complexes, the total number of propagation steps was 10000, thus the total propagation time for each time step were 200, 500 and 2000 a.u.respectively. For the Ag_8 complex, only two time steps were adopted, 0.02 and 0.2 a.u. and the corresponding number of time steps were 10000 and 4000 respectively. Fragment based Hirshfeld population and Becke population were calculated to analyze the evolution of electron density and energy on the oxygen molecule.

Chapter 3

Results

3.1 RT-TDDFT Results

3.1.1 Energy and Electron Density Evolution
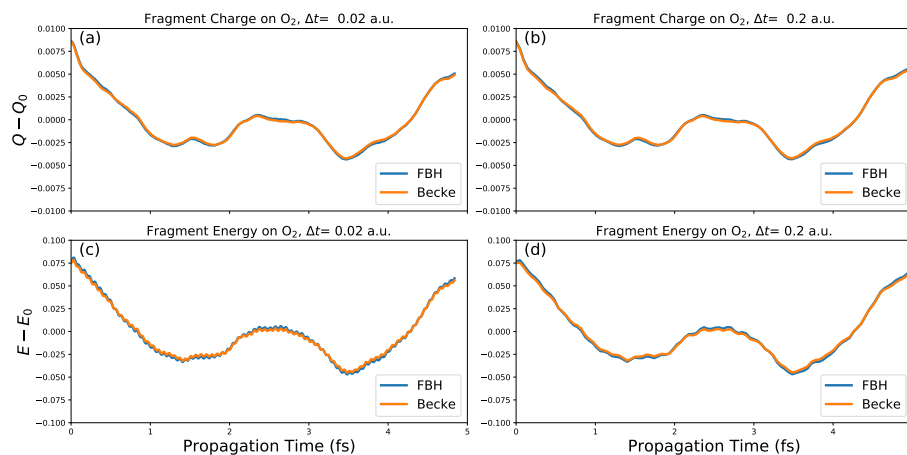
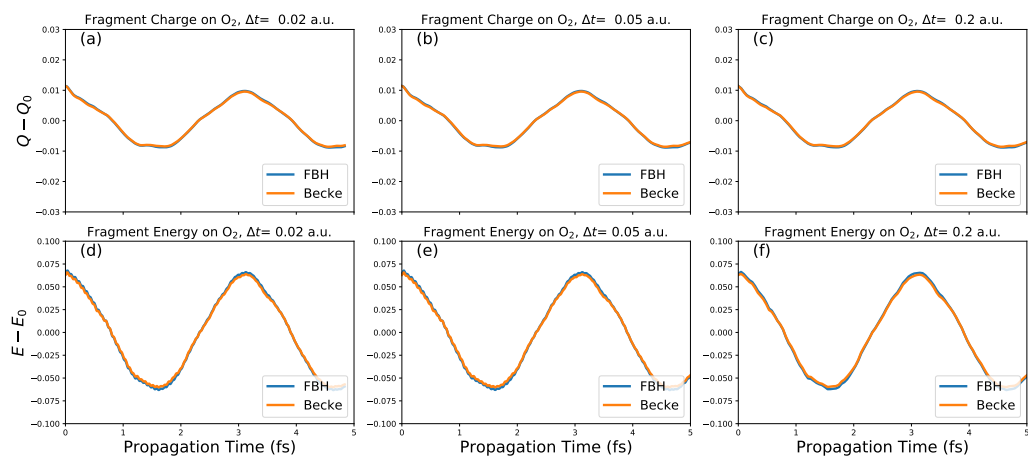Figure 3.1: Net charges (a-b) and energy (c-d) evolution of Ag_8-NC-O_2 with different time step.

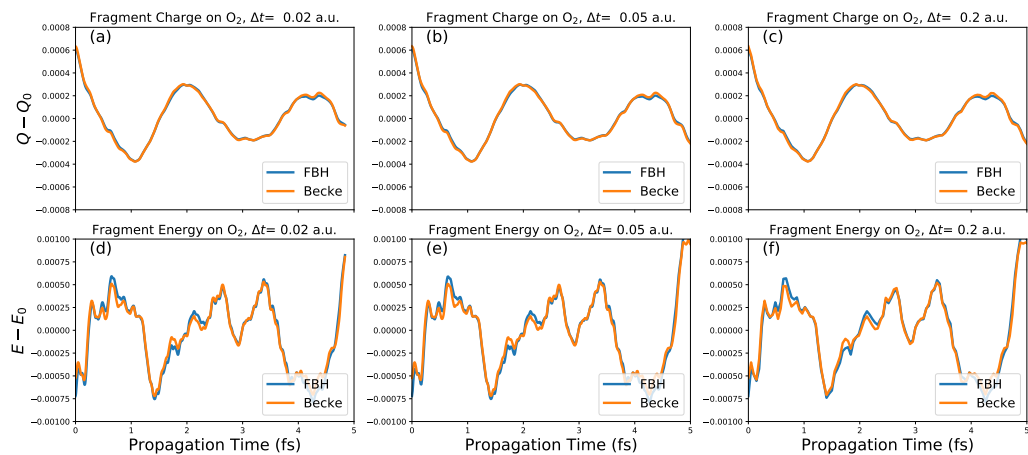Figure 3.2: Net charges (a-c) and energy (d-f) evolution of "top-parallel-long" Ag_4-NC-O_2 with different time step.

Figure 3.3: Net charges (a-c) and energy (d-f) evolution of Ag_4-NW-O_2 with different time step.

The energy and charge evolution curves for O_2 of Ag_8-NC-O_2, Ag_4-NC-O_2, Ag_4-NW-O_2 complexes are shown in Fig. 3.1, 3.2 and 3.3 respectively. (Note that the charge here refers to the net charges on the O_2 molecule.) For the Ag_4-NC-O_2 complexes, only the of result of "top-parallel-long" configuration is shown here due to its most significant net charge oscillation among all eight configurations. Looking at the curves of Ag_8-NC-O_2 and Ag_4-NC-O_2, clearly, the charge and energy fluctuate synchronously since the sign of charge and energy on O_2 are always the same. It is consistent with the fact that the energy of a system will decrease when additional electrons are added and vice versa. However, for Ag_4-NC-O_2 complex, it has a very different behavior shown in Fig. 3.3. Although, the overall shapes of charge evolution and energy evolution curve are quite similar, a phase difference of around 1.6 fs can be observed which is indicating that the charge and energy are out of sync to each other. It is a character of the indirect electron transfer mechanism (PHET). According to the PHET mechanism, the electrons in the occupied orbitals of Ag_4-NC are excited to its virtual orbital first and then undergo thermalization to Fermi-Dirac distribution through electron-electron scattering. During the electron-electron scattering process, the energy transfer should not be in sync to the electron transfer.

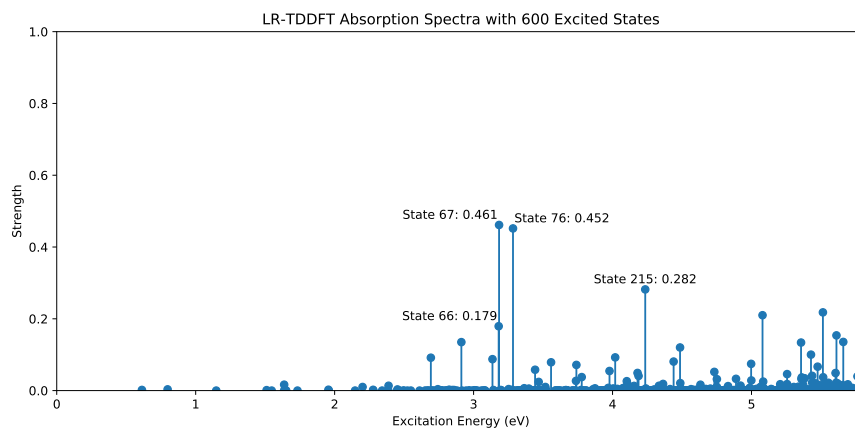## 3.2 LR-TDDFT Results

3.2.1 Absorption Spectra

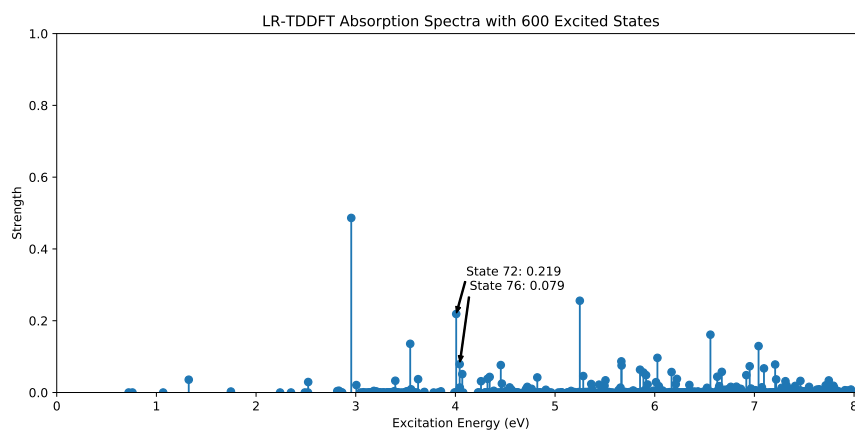Figure 3.4: LR-TDDFT absorption spectrum with 600 excited states for Ag$_8$-NC-O$_2$

Figure 3.5: LR-TDDFT absorption spectrum with 600 excited states for "top-parallel-long" Ag$_4$-NC-O$_2$

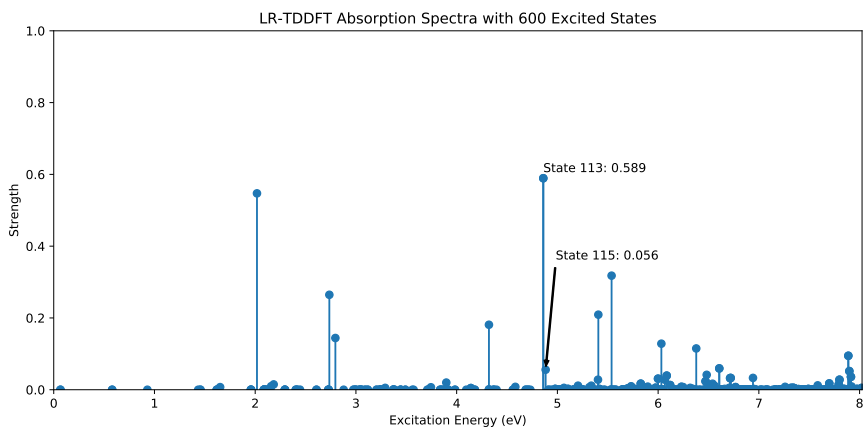LR-TDDFT Absorption Spectra with 600 Excited States

State 113: 0.589

State 115: 0.056

Figure 3.6: LR-TDDFT absorption spectrum with 600 excited states for Ag$_4$-NW-O$_2$

The absorption spectra with 600 excited states of three complexes solved by using LR-TDDFT method are shown in Fig. 3.4, 3.5 and 3.6 respectively. For Ag$_8$-NC-O$_4$ complex, the 67th, 67th, 76th and 215th excited states were picked out for further examination through looking at their NTOs due to their relative high oscillation strengths. Besides, 66th excited state is also selected because it is degenerate with 67th state.

For the same reason, the 15th, 72th and 76th excited state of Ag$_4$-NC-O$_2$ complex as well as the 113th and 115th of Ag$_4$-NW-O$_2$ complex are picked out.
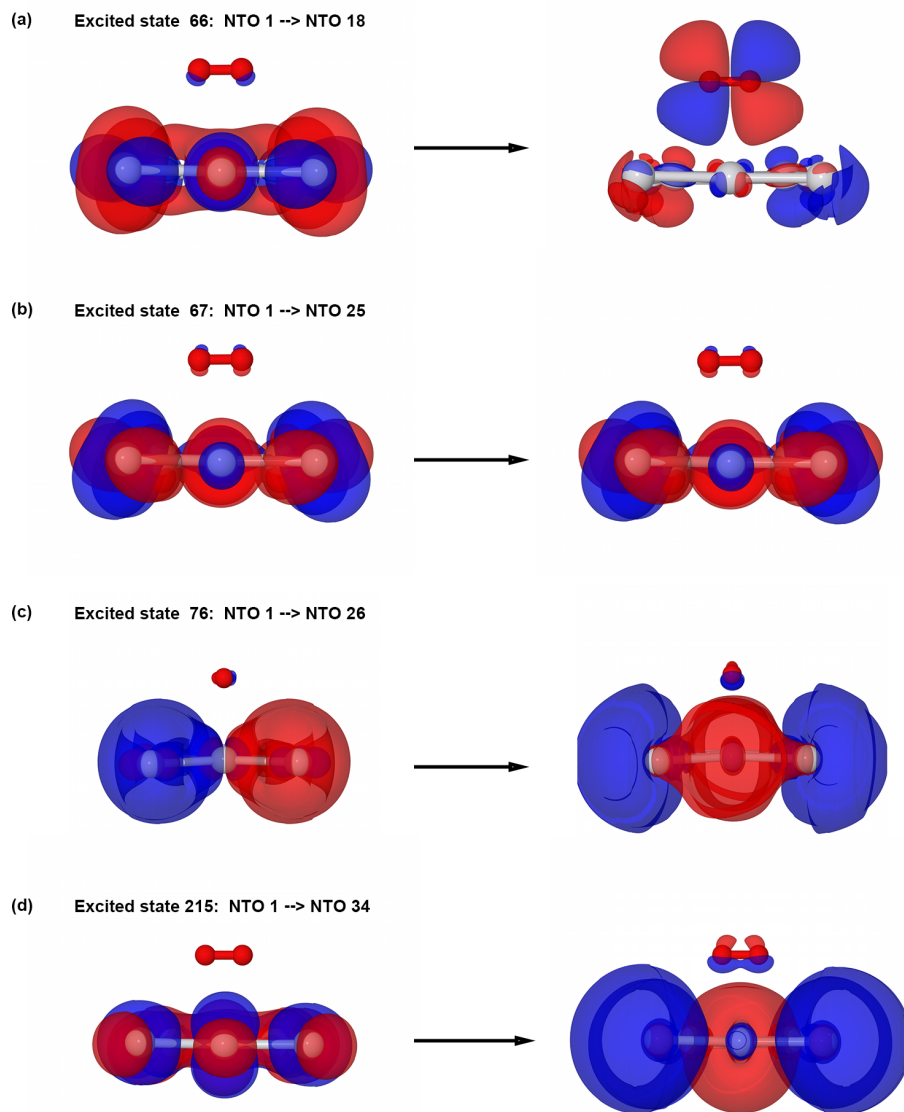
3.2.2   Natural Transition Orbitals Analysis

Figure 3.7: Selected natural transition orbitals of Ag$_8$-NC-O$_2$ (Isovalue=0.01 a.u.)

Table 3.1: Selected NTOs of Ag_8-NC-O_2

Excited state	NTO pair	Eigenvalues
66	$1 \rightarrow 18$	0.723
67	$1 \rightarrow 25$	0.296
76	$1 \rightarrow 26$	0.330
215	$1 \rightarrow 34$	0.314

For each excited state, the pair of NTOs with the largest eigenvalue were picked out and plotted, because the largest eigenvalue means that it plays the most important role. The selected NTOs of Ag_8-NC-O_2 complex mentioned in the previous section are shown in Fig. 3.7 and the corresponding eigenvalues are shown in Tab. 3.1. In Fig. 3.1(a), the hole is mainly locates on Ag while the particle is transferred to a delocalized π^* orbital on O_2. This is indicating that the 66th excited state is a charge-transfer excited state, to be more specific, it is a "$\pi \rightarrow \pi^*$" excitation. And it can be the evidence that DICT mechanism contributes part of the electron transfer during the decay of plasmon on Ag_8-NC-O_2 complex. However, the other NTO pairs show a different picture of hole and particle: both of the hole and the particle mainly locate on Ag. And especially in Fig. 3.1(c) and (d), the particle is more delocalized than the hole. It is reasonable to consider the 67th, 67th and 215th excited states are local excitations which are supporting the PHET mechanism. Overall, both of the characters of PHET and DICT mechanism show up in the excitation of Ag_8-NC-O_2 complex, however, the oscillation strength of the charge transfer state is much lower than any other state shown in Fig. 3.1. Therefore, PHET mechanism can be considered as the major pathway governing charge transfer in this complex..
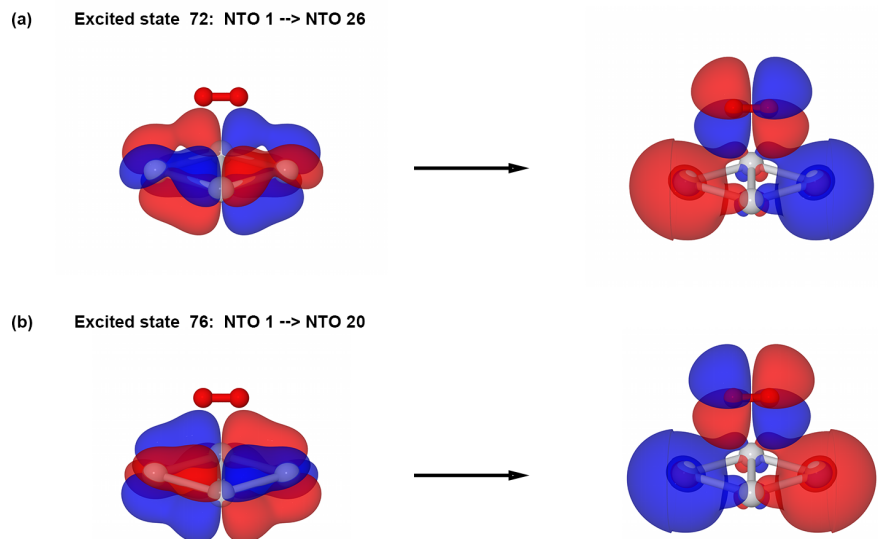
(a) Excited state 72: NTO 1 --> NTO 26

(b) Excited state 76: NTO 1 --> NTO 20

Figure 3.8: Selected natural transition orbitals of "top-parallel-long" Ag_4-NC-O_2 (Isovalue=0.01 a.u.)

Table 3.2: Selected NTOs of "top-parallel-long" Ag_4-NC-O_2

Excited state	NTO pair	Eigenvalues
72	$1 \rightarrow 26$	0.356
76	$1 \rightarrow 20$	0.630

For the "top-parallel-long" Ag_4-NC-O_2 complex, it is clear to see that both of the excited states shown in Fig. 3.8 refers to the "$\pi \rightarrow \pi^*$" excitation. It is a charge transfer from the occupied orbital of Ag_4 to the virtual orbital the O_2 molecule. However, due to the relative low oscillation strengths of the selected excited states, the DICT mechanism is not that significant. As a result, it is reasonable to consider PHET mechanism as the one dominating the charge transfer process while both mechanisms are involved.
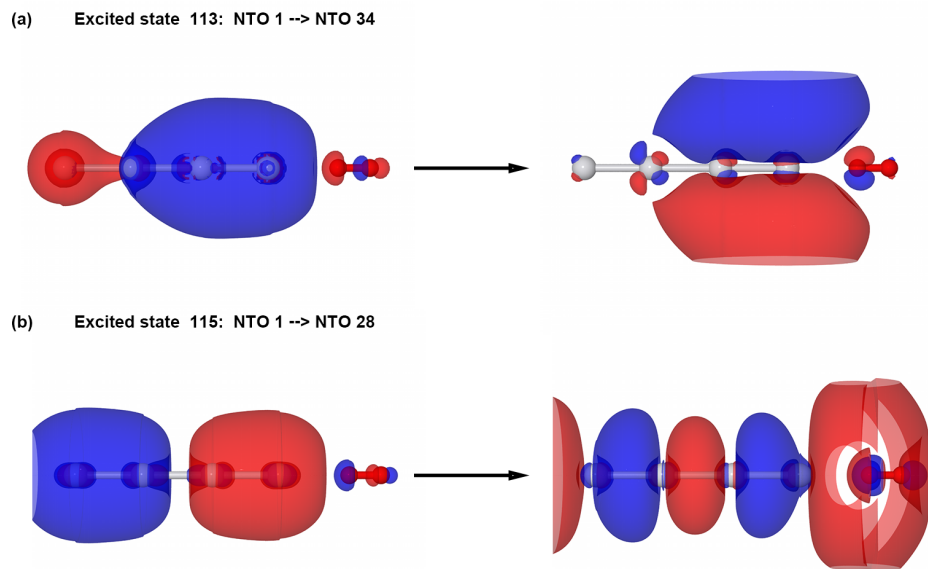
(a) Excited state 113: NTO 1 --> NTO 34

(b) Excited state 115: NTO 1 --> NTO 28

Figure 3.9: Selected natural transition orbitals of Ag_4-NW-O_2 (Isovalue=0.01 a.u.)

Table 3.3: Selected NTOs of Ag_4-NW-O_2

Excited state	NTO pair	Eigenvalues
113	$1 \rightarrow 34$	0.267
115	$1 \rightarrow 28$	0.464

For the Ag_4-NW-O_2 complex, in Fig. 3.8, the holes of two excited states are mainly locating on Ag_4-NW. The particle of the 113th state still mainly locate on Ag but it becomes much more delocalized than the hole. Thus, it can be considered as a local excitation. While, for the 115th excited state, the particle becomes extreme delocalized throughout the whole complex. The virtual NTO of Ag_4 mixes with that of O_2 so that it is possible for the electron to transfer from Ag_4 to O_2 directly. Nonetheless, the small oscillation strength of 115th excited state, 0.056, indicates that it can not the major electron transfer mode.

25

Chapter 4

Conclusions

By comparing the the RT-TDDFT and LR-TDDFT results of all complexes in this study, one can observe that the both of local excitations and charge transfer excitation between Ag NP and O_2 exist in the excitation process. The existence of direct charge transfer shown in this work is consistent with experimental results. But the local excitation still holds the major contribution to the overall excitation while charge-transfer excitation only has limited contribution for the Ag-NP-O_2 system.

Besides, by comparing the results of different complexes or configurations, it can be seen that the parallel configuration tend to make the charge-transfer excitation more significant. The potential reason is the relative larger orbital overlap between the orbitals of two fragments.
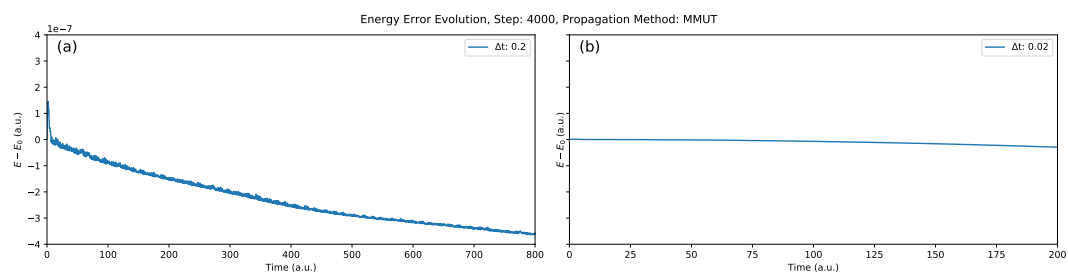
Appendix A

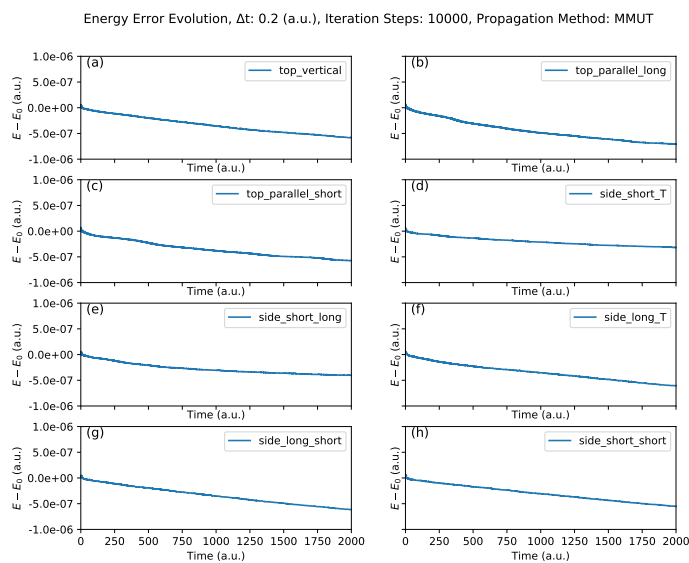# Figures

Figure A.1: RT-TDDFT energy conservation for Ag$_8$-NC-O$_2$

Energy Error Evolution, Δt: 0.2 (a.u.), Iteration Steps: 10000, Propagation Method: MMUT

Figure A.2: RT-TDDFT energy conservation for Ag_4-NC-O_2 with a time step of 0.2 a.u.

Energy Error Evolution, Δt: 0.05 (a.u.), Iteration Steps: 10000, Propagation Method: MMUT
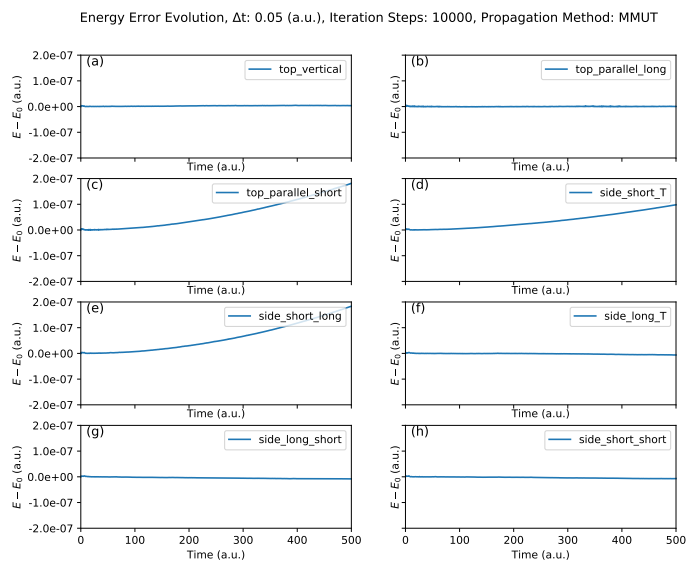
Figure A.3: RT-TDDFT energy conservation for Ag_4-NC-O_2 with a time step of 0.05 a.u.

Energy Error Evolution, Δt: 0.02 (a.u.), Iteration Steps: 10000, Propagation Method: MMUT
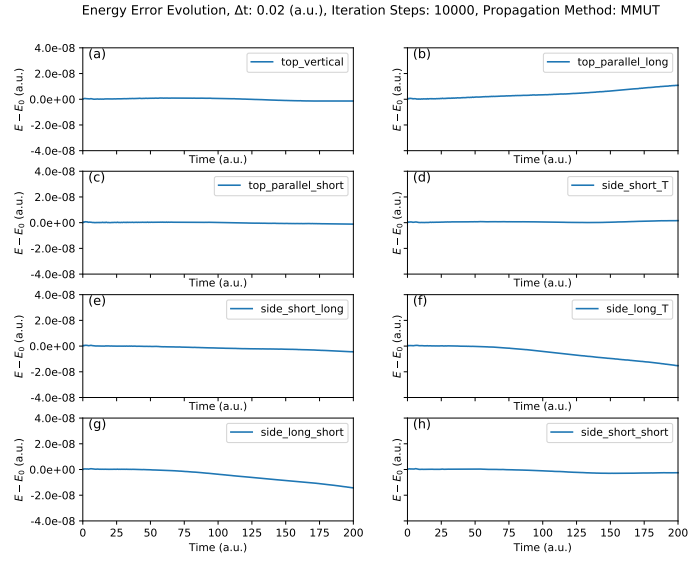
Figure A.4: RT-TDDFT energy conservation for Ag_4-NC-O_2 with a time step of 0.02 a.u.

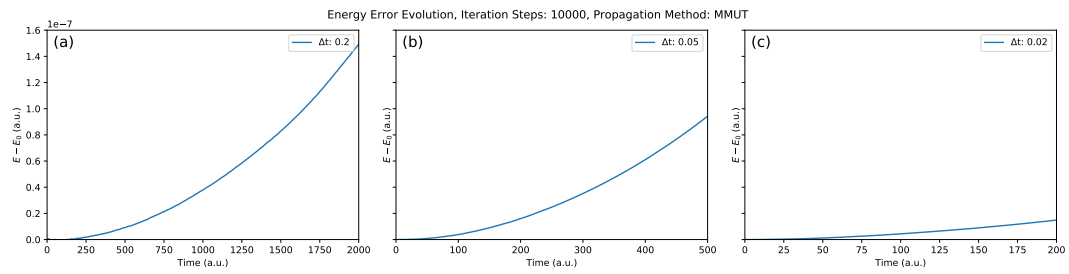Energy Error Evolution, Iteration Steps: 10000, Propagation Method: MMUT

Figure A.5: RT-TDDFT energy conservation for Ag_4-NW-O_2

29

Bibliography

[1] Günter Schmid. Chapter 1 - general features of metal nanoparticles physics and chemistry. In B. CORAIN, G. SCHMID, and N. TOSHIMA, editors, *Metal Nanoclusters in Catalysis and Materials Science*, pages 3 – 20. Elsevier, Amsterdam, 2008.

[2] Susie Eustis and Mostafa A. El-Sayed. Why gold nanoparticles are more precious than pretty gold: Noble metal surface plasmon resonance and its enhancement of the radiative and nonradiative properties of nanocrystals of different shapes. *Chem. Soc. Rev.*, 35:209–217, 2006.

[3] Matthew J. Kale, Talin Avanesian, and Phillip Christopher. Direct photocatalysis by plasmonic nanostructures. *ACS Catalysis*, 4(1):116–128, 2014.

[4] Jhon Quiroz, Eduardo CM Barbosa, Thaylan P Araujo, Jhonatan L Fiorio, Yi-Chi Wang, Yi-Chao Zou, Tong Mou, Tiago V Alves, Daniela C de Oliveira, Bin Wang, et al. Controlling reaction selectivity over hybrid plasmonic nanocatalysts. *Nano letters*, 18(11):7289–7297, 2018.

[5] Lasse Jensen, Christine M. Aikens, and George C. Schatz. Electronic structure methods for studying surface-enhanced raman scattering. *Chem. Soc. Rev.*, 37:1061–1073, 2008.

[6] Seth M. Morton and Lasse Jensen. Understanding the molecule—surface chemical coupling in sers. *Journal of the American Chemical Society*, 131(11):4090–4098, 2009.

[7] Akira Fujishima and Kenichi. Honda. Electrochemical photolysis of water at a semiconductor electrode. *Nature*, 238(5358):37–38, 1972.

[8] Akihiro Furube and Shuichi Hashimoto. Insight into plasmonic hot-electron transfer and plasmon molecular drive: new dimensions in energy conversion and nanofabrication. *NPG Asia Materials*, 9(12):e454–e454, 2017.

[9] Umar Aslam, Vishal Govind Rao, Steven Chavez, and Suljo Linic. Catalytic conversion of solar to chemical energy on plasmonic metal nanostructures. *Nature Catalysis*, 1(9):656–665, 2018.

[10] César Clavero. Plasmon-induced hot-electron generation at nanoparticle/metal-oxide interfaces for photovoltaic and photocatalytic devices. *Nature Photonics*, 8(2):95, 2014.

[11] Svetlana V Boriskina, Hadi Ghasemi, and Gang Chen. Plasmonic materials for energy: From physics to applications. *Materials Today*, 16(10):375–386, 2013.

[12] Eduardo CM Barbosa, Jhonatan L Fiorio, Tong Mou, Bin Wang, Liane M Rossi, and Pedro HC Camargo. Reaction pathway dependence in plasmonic catalysis: hydrogenation as a model molecular transformation. *Chemistry–A European Journal*, 24(47):12330–12339, 2018.

[13] K. Wu, J. Chen, J. R. McBride, and T. Lian. Efficient hot-electron transfer by a plasmon-induced interfacial charge-transfer transition. *Science*, 349(6248):632–635, 2015.

[14] Gregory V. Hartland. Optical studies of dynamics in noble metal nanostructures. *Chemical Reviews*, 111(6):3858–3887, 2011.

[15] Calvin Boerigter, Umar Aslam, and Suljo Linic. Mechanism of charge transfer from plasmonic nanostructures to chemically attached materials. *ACS Nano*, 10(6):6108–6115, 2016.

[16] Krystyna Kolwas. Decay dynamics of localized surface plasmons: Damping of coherences and populations of the oscillatory plasmon modes. *Plasmonics*, 14(6):1629–1637, 2019.

[17] Yuchao Zhang, Shuai He, Wenxiao Guo, Yue Hu, Jiawei Huang, Justin R. Mulcahy, and Wei David Wei. Surface-plasmon-driven hot electron photochemistry. *Chemical Reviews*, 118(6):2927–2954, 2018.

[18] Benjamin Foerster, Anneli Joplin, Katharina Kaefer, Sirin Celiksoy, Stephan Link, and Carsten Sönnichsen. Chemical interface damping depends on electrons reaching the surface. *ACS Nano*, 11(3):2886–2893, 2017.

[19] Louis Brus. Noble metal nanocrystals: Plasmon electron transfer photochemistry and single-molecule raman spectroscopy. *Accounts of Chemical Research*, 41(12):1742–1749, 2008.

[20] Umar Aslam, Suljo Linic, Calvin Boerigter, and Matthew Morabito. Photochemical transformations on plasmonic metal nanoparticles. *Nature Materials*, 14(6):567–576, 2015.

[21] Siwei Li, Peng Miao, Yuanyuan Zhang, Jie Wu, Bin Zhang, Yunchen Du, Xijiang Han, Jianmin Sun, and Ping Xu. Recent advances in plasmonic nanostructures for enhanced photocatalysis and electrocatalysis. *Advanced Materials*, page 2000086, 2020.

[22] Bhogeswararao Seemala, Andrew J. Therrien, Minhan Lou, Kun Li, Jordan P. Finzel, Ji Qi, Peter Nordlander, and Phillip Christopher. Plasmon-mediated catalytic o2 dissociation on ag nanostructures: Hot electrons or near fields? *ACS Energy Letters*, 4(8):1803–1809, 2019.

[23] Phillip Christopher, Hongliang Xin, and Suljo Linic. Visible-light-enhanced catalytic oxidation reactions on plasmonic silver nanostructures. *Nature chemistry*, 3(6):467, 2011.

[24] Phillip Christopher, Hongliang Xin, Andiappan Marimuthu, and Suljo Linic. Singular characteristics and unique chemical bond activation mechanisms of photocatalytic reactions on plasmonic nanostructures. *Nature Materials*, 11(12):1044 – 1050, 2012.

[25] Fenglei Shi, Jing He, Baiyu Zhang, Jiaheng Peng, Yanling Ma, Wenlong Chen, Fan Li, Yong Qin, Yang Liu, Wen Shang, Peng Tao, Chengyi Song, Tao Deng, Xiaofeng Qian, Jian Ye, and Jianbo Wu. Plasmonic-enhanced oxygen reduction reaction of silver/graphene electrocatalysts. *Nano Letters*, 19(2):1371–1378, 2019.

[26] Linlin Zhao, Lasse Jensen, and George C Schatz. Pyridine-ag20 cluster: a model system for studying surface-enhanced raman scattering. *Journal of the American Chemical Society*, 128(9):2911—2919, 2006.

[27] Bo Peng, David B. Lingerfelt, Feizhi Ding, Christine M. Aikens, and Xiaosong Li. Real-time tddft studies of exciton decay and transfer in silver nanowire arrays. *The Journal of Physical Chemistry C*, 119(11):6421–6427, 2015.

[28] Jun Yan, Karsten W. Jacobsen, and Kristian S. Thygesen. First-principles study of surface plasmons on ag(111) and h/ag(111). *Phys. Rev. B*, 84:235430, 2011.

[29] S Kümmel, K Andrae, and P-G Reinhard. Collectivity in the optical response. of small metal clusters. *Applied Physics B*, 73(4):293–297, 2001.

[30] Gyun-Tack Bae and Christine M Aikens. Time-dependent density functional theory studies of optical properties of au nanoparticles: Octahedra, truncated octahedra, and icosahedra. *The Journal of Physical Chemistry C*, 119(40):23127–23137, 2015.

[31] Christine M Aikens, Shuzhou Li, and George C Schatz. From discrete electronic states to plasmons: Tddft optical absorption properties of ag n (n= 10, 20, 35, 56, 84, 120) tetrahedral clusters. *The Journal of Physical Chemistry C*, 112(30):11272–11279, 2008.

[32] Hannah E Johnson and Christine M Aikens. Electronic structure and tddft optical absorption spectra of silver nanorods. *The Journal of Physical Chemistry A*, 113(16):4445–4450, 2009.

[33] Gyun-Tack Bae and Christine M Aikens. Time-dependent density functional theory studies of optical properties of ag nanoparticles: octahedra, truncated octahedra, and icosahedra. *The Journal of Physical Chemistry C*, 116(18):10356–10367, 2012.

[34] Emilie B Guidez and Christine M Aikens. Diameter dependence of the excitation spectra of silver and gold nanorods. *The Journal of Physical Chemistry C*, 117(23):12325–12336, 2013.

[35] Yihan Shao, Zhengting Gan, Evgeny Epifanovsky, T.B. Gilbert, Michael Wormit, Joerg Kussmann, W Lange, Andrew Behn, Jia Deng, Xintian Feng, and et al. Advances in molecular quantum chemistry contained in the q-chem 4 program package. *Molecular Physics*, 113(2):184–215, 2015.

[36] Pierre Hohenberg and Walter Kohn. Inhomogeneous electron gas. *Physical review*, 136(3B):B864, 1964.

[37] Walter Kohn and Lu Jeu Sham. Self-consistent equations including exchange and correlation effects. *Physical review*, 140(4A):A1133, 1965.

[38] R.G. Parr and Y. Weitao. *Density-Functional Theory of Atoms and Molecules*. International Series of Monographs on Chemistry. Oxford University Press, 1994.

[39] Erich Runge and E. K. U. Gross. Density-functional theory for time-dependent systems. *Phys. Rev. Lett.*, 52:997–1000, 1984.

[40] Mark E Casida. Time-dependent density functional response theory for molecules. In *Recent Advances In Density Functional Methods: (Part I)*, pages 155–192. World Scientific, 1995.

[41] So Hirata and Martin Head-Gordon. Time-dependent density functional theory within the tamm–dancoff approximation. *Chemical Physics Letters*, 314(3):291 – 299, 1999.

[42] Ying Zhu and John M. Herbert. Self-consistent predictor/corrector algorithms for stable and efficient integration of the time-dependent kohn-sham equation. *The Journal of Chemical Physics*, 148(4):044117, 2018.

[43] Richard L. Martin. Natural transition orbitals. *The Journal of Chemical Physics*, 118(11):4775–4777, 2003.

[44] F. L. Hirshfeld. Bonded-atom fragments for describing molecular charge densities. *Theoretica Chimica Acta*, 44(2):129–138, 1977.

[45] A. D. Becke. A multicenter numerical integration scheme for polyatomic molecules. *The Journal of Chemical Physics*, 88(4):2547–2553, 1988.

[46] Ye Mei, Andrew C. Simmonett, Frank C. Pickard, Robert A. DiStasio, Bernard R. Brooks, and Yihan Shao. Numerical study on the partitioning of the molecular polarizability into fluctuating charge and induced atomic dipole contributions. *The Journal of Physical Chemistry A*, 119(22):5865–5882, 2015.

[47] Roger C. Baetzold. Silver–water clusters: A theoretical description of agn(h2o)m for n = 1–4; m = 1–4. *The Journal of Physical Chemistry C*, 119(15):8299–8309, 2015.

[48] Feizhi Ding, Emilie B. Guidez, Christine M. Aikens, and Xiaosong Li. Quantum coherent plasmon in silver nanowires: A real-time tddft study. *The Journal of Chemical Physics*, 140(24):244705, 2014.

[49] John P. Perdew, Kieron Burke, and Matthias Ernzerhof. Generalized gradient approximation made simple. *Phys. Rev. Lett.*, 77:3865–3868, 1996.

[50] D Andrae, U Haeussermann, M Dolg, H Stoll, and H Preuss. Energy-adjustedab initio pseudopotentials for the second and third row transition elements. *Theoretica chimica acta*, 77(2):123–141, 1990.

[51] Qiming Sun, Timothy C Berkelbach, Nick S Blunt, George H Booth, Sheng Guo, Zhendong Li, Junzi Liu, James D McClain, Elvira R Sayfutyarova, Sandeep Sharma, et al. Pyscf: the python-based simulations of chemistry framework. *Wiley Interdisciplinary Reviews: Computational Molecular Science*, 8(1):e1340, 2018.